Proceedings of the
Annual Stability Conference
Structural Stability Research Council
Nashville, Tennessee, March 24-27, 2015

On the Mechanics of Local-Distortional Interaction in Lipped Channel Thin-Walled Columns

André D. Martins[1], Dinar Camotim[1], Pedro B. Dinis[1], Paulo Providência[2]

Abstract

The objective of this paper is to present and discuss numerical (GBT-based) results concerning the geometrically non-linear response of thin-walled lipped channel columns experiencing local-distortional (L-D) interaction that will shed fresh light on the mechanics underlying this coupling phenomenon. These results, obtained through GBT elastic post-buckling analyses, provide the evolution, along given equilibrium paths, of the column (i) deformed configuration, expressed in modal form, (ii) relevant displacement profiles, and (iii) stress distributions. Taking full advantage of the GBT unique modal features, it becomes possible to unveil the most relevant behavioral/mechanical features associated with the occurrence of L-D interaction. Particular attention is devoted to the structural interpretation/explanation of the quantitative and qualitative differences exhibited by the column post-buckling behaviors associated with (i) "pure"/individual local and distortional deformations (*e.g.*, Silvestre & Camotim 2006), and (ii) the occurrence L-D interaction stemming from either the closeness between the local and distortional critical buckling stresses ("true interaction") or from a secondary bifurcation phenomenon ("secondary-bifurcation interaction") – Martins *et al.* (2014a,b). Finally, it is expected that the outcome of this investigation will have impact on the improvement/development of existing/new design approaches, based on the Direct Strength Method (DSM), against failures caused by the above two types of L-D interactive behavior.

1. Introduction

Commonly used cold-formed steel structural systems are very often formed by slender open-section thin-walled members, which means that their structural behavior and ultimate strength are frequently governed by instability effects possibly involving cross-section deformation, namely local (L), distortional (D) and/or global (G) buckling. However, in order to assess the structural efficiency of slender thin-walled members it is not enough obtain in-depth information (buckling and post-buckling) about their "pure"/individual (L, D and/or G) behaviors, since any interaction involving these three instability phenomena may occur, namely: L-G, L-D, D-G or L-D-G interaction – however, this

[1] ICIST, CEris, DECivil, Instituto Superior Técnico, Universidade de Lisboa, Portugal. <andrerdmartins@ist.utl.pt>, <dcamotim@civil.ist.utl.pt> and <dinis@civil.ist.utl.pt>

[2] Department of Civil Engineering, INESC, University of Coimbra, Portugal. <provid@dec.uc.pt>

work deals solely with L-D interaction[3]. The main challenge that the technical/scientific community faces is knowing when these effects are important, *i.e.*, assessing their relevance. In fact, neglecting any of these interaction phenomena may lead to unacceptably low reliability indices, *i.e.*, to a high likelihood of reaching unsafe designs.

Traditionally, the non-linear behavior of thin-walled members could only be rigorously assessed by resorting (i) to shell finite element simulations (*e.g.*, Dinis *et al*. 2007), which are time-consuming and computationally costly, or, to a smaller extent, (ii) to spline finite element analyses (*e.g.*, Prola & Camotim 2002), both providing outputs that are not easy to apprehend. However, in the last decade this situation has been altered, due to the formulation of a geometrically elastic non-linear Generalized Beam Theory (GBT) by Silvestre & Camotim (2003), which emerged as a very promising alternative to obtain similarly accurate results (equilibrium equations valid in large deformation range) in a much more efficient (drastic reduction of the number of d.o.f. required) and clarifying (structurally meaningful modal d.o.f.) manner. By performing GBT-based geometrically non-linear imperfect analyses (GNIA) of prismatic thin-walled members, it becomes possible to identify and quantify the contributions of the various deformation modes to the member structural response under consideration, a feature that enables a much more in-depth understanding of that same response, thus providing a clearer and deeper understanding on the mechanical aspects involved. Regarding the elastic non-linear GBT formulations to analyze cold-formed steel members (isotropic materials), it is worth noting the investigations reported by (i) Silvestre & Camotim (2003, 2006) on the local and distortional post-buckling behavior of uniformly compressed columns with "plain" (*i.e.*, without intermediate stiffeners) (i_1) lipped channel and Z-sections, and (i_2) web-flange stiffened lipped channel sections, (ii) Silvestre & Camotim (2004a) on the distortional post-buckling analysis of Z-sections beams, (iii) Bebiano *et al*. (2005), who reported an investigation on the distortional post-buckling behavior of cold-formed steel lipped channel columns with several intermediate and/or end stiffeners, and, recently, (iii) Basaglia *et al*. (2014), who investigated the influence of the cross-section geometry on the distortional post-buckling of lipped channel and hat-section simply supported columns[4]. Still regarding the application of GBT to analyze the non-linear response of cold-formed steel structures, (i) Basaglia *et al*. (2011) reported an investigation on the effect of non-standard support conditions on the post-buckling behavior of columns and beams, and (ii) extended the GBT formulation to the analysis of thin-walled frames (*e.g.*, Basaglia *et al*. 2013), by developing a "joint element" that guarantees the compatibility between connected members. Recently, Silva (2013) developed and implemented a GBT-beam finite element to analyze the post-buckling behavior of laminated FRP (Fibre Reinforced Polymers) composite thin-walled members with arbitrary cross-section shapes (*e.g.*, Silva *et al*. 2011), based on a beam finite element implementation of a geometrically non-linear GBT formulation derived a few years earlier by Silvestre & Camotim (2004b) and Silvestre (2005). As far as isotropic thin-walled members affected by L-D interaction are concerned, and to the authors' best knowledge, the only GBT-based numerical post-buckling results available were obtained by Silvestre & Camotim (2004c) for simply supported lipped channel columns with almost coincident local and distortional critical buckling stresses.

Previous work by the authors (Martins *et al*. 2014a,b), based on shell finite element analysis, showed that cold-formed steel columns may be affected by two types of L-D interaction, namely (i) one due to the

[3] Although this work deals exclusively with L-D interaction in cold-formed steel columns, these interaction phenomena are not restricted to these structural systems. Results reported by Silvestre *et al*. (2008) showed both experimental and numerical evidence of L-D interaction in CFRP ("Carbon-Fiber-Reinforced Polymer")-strengthened cold-formed steel lipped channel columns.

[4] Aside from the pioneering work of Miosga (1976), nowadays only with historical interest.

closeness between the local and distortional critical buckling stresses, denoted as "true L-D interaction"[5], and (ii) the other caused by a "secondary (L or D) bifurcation", which occurs when the local and distortional critical buckling stresses are not so close and stems from the high/moderate local/distortional post-critical strength reserve – the latter occurs mainly because thin-walled systems are made of high-strength steels, whose very high yield stresses leave enough "room" for the occurrence of L-D interaction.

The objective of this paper is to present and discuss numerical (GBT-based) results concerning the geometrically non-linear response of thin-walled lipped channel columns experiencing local-distortional (L-D) interaction, which are expected to shed fresh light on the mechanics underlying this coupling phenomenon. The above results, obtained through GBT elastic post-buckling analyses, provide the evolution, along given equilibrium paths, of the column (i) deformed configuration, expressed in modal form, (ii) relevant displacement profiles, and (iii) stress distributions. For validation purposes the GBT-based analyses are compared with values yielded by shell finite element analyses performed in the code ABAQUS (Simulia Inc, 2008). Taking full advantage of the GBT unique modal features, it becomes possible to unveil the most relevant behavioral/mechanical features associated with the occurrence of L-D interaction. Special attention is devoted to structurally interpreting/explaining the quantitative and qualitative differences exhibited by the column post-buckling behaviors associated with (i) "pure"/individual local and distortional deformations (*e.g.*, Silvestre & Camotim 2006), and (ii) the occurrence of either "true L-D interaction" or "secondary-bifurcation L-D interaction" (Martins *et al.* 2014a,b). Finally, it is also expected that the outcome of this investigation study will have impact on the improvement/development of existing/new design approaches, based on the Direct Strength Method (DSM), against failures caused by the above two types of L-D interactive behavior.

2. Brief Overview of the Non-Linear GBT Formulation

The performance of a GBT-based analysis involves two main tasks, namely (i) a *cross-section analysis*, concerning the identification of the deformation modes and evaluation of the corresponding modal mechanical properties, and (ii) a *member analysis* (in this paper: elastic buckling and post-buckling analyses), which consists of solving a differential equilibrium equation system. Next, the main aspects involved in each of these tasks, when investigating the elastic post-buckling behavior of lipped channel columns affected by local-distortional interaction, are briefly addressed.

2.1 Cross-Section Analysis

Consider a reference system where x, s and z denote coordinates along the member length, cross-section mid-line and wall thickness, where u, v and w are the corresponding displacement fields. According to GBT, the member mid-surface displacement field considers the variable separation

$$u(x,s)=u_k(s)\phi_{k,x}(x) \qquad v(x,s)=v_k(s)\phi_k(x) \qquad w(x,s)=w_k(s)\phi_k(x) \tag{1}$$

where (i) $(.)_{,x}\equiv d(.)/dx$, (ii) the summation convention of Einstein applies to subscript k, (iii) $\phi_k(x)$ are the modal displacement amplitude functions defined along the member length (*member analysis* unknowns), and (iv) functions $u_k(s)$, $v_k(s)$ and $w_k(s)$ are the displacements profiles associated with the deformation mode k, yielded by the *cross-section analysis*.

The GBT cross-section analysis involves a lengthy and fairly complex set of operations, which has been described in detail in the literature (*e.g.*, Silvestre & Camotim 2003 and Silvestre 2005).

[5] The columns analyzed by Silvestre & Camotim (2004c) fall into this category.

Nevertheless, the key aspects concerning the procedures involved, for unbranched open cross-sections, are pointed out next:

(i) The member cross-section (with *n* walls) is discretized into (i_1) *n*+1 natural nodes (wall edges) and (i_2) *m* intermediate nodes (located within the walls).

(ii) The deformations modes are divided into three sets, namely the (ii_1) *conventional* modes (originally considered by Schardt 1989), (ii_2) *shear* modes, and (ii_3) *transverse extension* modes – the last two sets were first introduced by Silvestre & Camotim (2003).

(iii) The *conventional* modes constitute the core of GBT, are based on Vlasov's assumptions of null membrane shear strains ($\gamma_{xs}^{M} = 0$) and transverse extensions ($\varepsilon_{ss}^{M} = 0$), and can be subdivided into (iii_1) *global* modes (cross-section in-plane rigid-boy motions: axial extension, major/minor-axis bending and torsion), (iii_2) *distortional* modes (involving warping and transverse wall bending) and (iii_3) *local* modes (associated with only transverse wall bending).

(iv) The *shear* modes concern exclusively the non-linear variation of the warping displacements along the cross-section wall mid-lines. They are obtained by imposing unit warping displacements $u(s)$ and null membrane transverse ($v(s)$) and flexural ($w(s)$) displacements at each natural and intermediate node – this means that the shear modes do not comply with Vlasov's assumption.

(v) Finally, the *transverse extension* modes involve only in-plane displacements ($u(s)=0$) and are characterized by non-null membrane transverse extensions ($\varepsilon_{ss}^{M} \neq 0$). They are obtained by imposing unit membrane transverse displacements $v(s)$ and null warping displacements $u(s)$ at each natural and intermediate node.

Figure 1 shows the GBT discretization adopted in this work, which (i) comprise 17 (6 natural and 11 intermediate) nodes, and (ii_1) leads to 17 conventional deformation modes (4 global, 2 distortional and 11 local), (ii_2) 14 shear modes and (ii_3) 14 transverse extension modes. The main features of the most relevant ones (5 conventional, 2 shear and 1 transverse extension – numbered sequentially in this order), *i.e.*, with significant contributions to the member structural response, are also displayed in Fig.1.

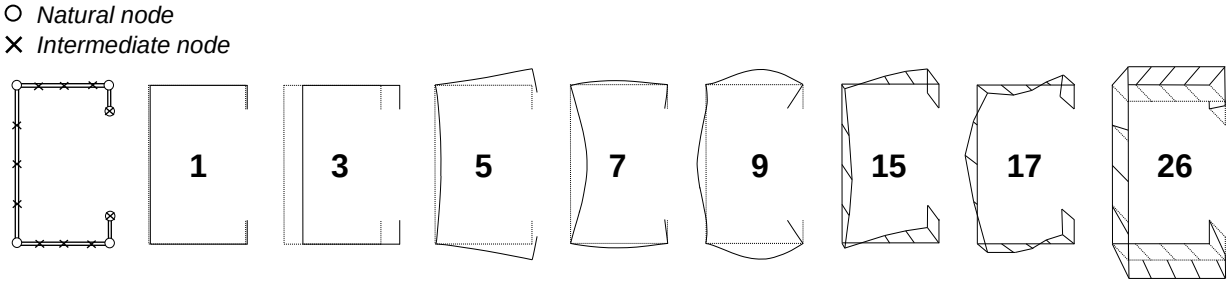

Figure 1: (i) In-plane deformed configurations of the most relevant conventional and transverse extension modes, and (ii) warping displacements of the most relevant shear modes, for lipped channels.

2.2 Member Analysis

After performing the cross-section analysis, the displacement fields of each deformation mode are known and the determination of the member post-buckling behavior involves the solution of the non-linear differential equilibrium equations (one per deformation mode) given by Silvestre & Camotim (2006),

$$C_{kh}\left(\phi_k-\bar{\phi}_k\right)_{,xxxx}-D_{kh}\left(\phi_k-\bar{\phi}_k\right)_{,xx}+B_{kh}\left(\phi_k-\bar{\phi}_k\right)-C_{kjh}\left(\phi_{k,xx}\phi_{j,x}-\bar{\phi}_{k,xx}\phi_{j,x}\right)_{,x}+\frac{1}{2}C_{hjk}\left(\phi_{k,x}\phi_{j,x}-\bar{\phi}_{k,x}\bar{\phi}_{j,x}\right)_{,xx}+$$
$$+\frac{1}{2}C_{kijh}\left(\phi_{k,x}\phi_{i,x}\phi_{j,x}-\bar{\phi}_{k,x}\bar{\phi}_{i,x}\phi_{j,x}\right)_{,x}+h.o.t.=q_h \qquad (2)$$

where (i) $\bar{\phi}_k$ is the modal amplitude function associated to deformation mode k, describing the initial geometrical imperfections (similar to Eq. (1)), (ii) q_h are the modal distributed loads, (iii) C_{kh}, B_{kh}, D_{kh} are second-order tensors defining modal mechanical properties characterizing the cross-section linear behavior, (iv) C_{kjh}, C_{kijh} are third and fourth-order tensors (note that there are also higher order terms, not shown in Eq. (2)), associated with the geometrically non-linear behavior – the expressions providing these tensor components can be found in Silvestre & Camotim (2003). The global modes **1**-**4**, *i.e.*, axial extension (C_{11}≡axial stiffness), major and minor-axis bending (C_{22} and C_{33}≡bending stiffness), and torsion (C_{44}≡warping torsion stiffness; D_{44}≡St. Venant torsional stiffness) have B_{kh}=0, as only cross-section rigid-body motions are involved. Since the distortional and local modes (k≥5) exhibit (i) primary and secondary warping displacements and/or (ii) cross-section in-plane deformation, they exhibit non-null C_{kh}, B_{kh}, and D_{kh} components with no obvious mechanical meaning. This lack of physical meaning is shared by all higher order mechanical tensors, even those associated with global modes.

The solution of (2), (i) together with (i) the appropriate support conditions and (ii) considering any selected subset of deformations modes, can be obtained by means of a GBT-based beam finite element formulation similar to that adopted by Basaglia *et al*. (2011), which is akin (but not identical) to the one developed by Silvestre & Camotim (2003). The main steps involved this formulation are briefly described next:

(i) Approximate the modal amplitude functions $\phi_k(x)$ by means of linear combinations of (i_1) Lagrange cubic polynomial primitives, for the deformations modes involving only warping displacements (*i.e.*, axial extension and shear modes), and (i_2) Hermite cubic polynomials, for the remaining conventional deformation modes and transverse extension modes.

(ii) The solution of the system of non-linear algebraic equations is obtained through an incremental-iterative technique based on (ii_1) Newton-Raphson's method and (ii_2) a load or arc-length control strategy (both strategies were implemented) – more details concerning the numerical implementation of the GBT non-linear formulation can be found in Clarke & Hancock (1990) and Crisfield (2001).

3. GBT Buckling Analysis – Column Geometry Selection

In order to investigate the mechanics of the geometrically non-linear response of thin-walled columns experiencing L-D interaction, it is indispensable to begin by selecting column geometries (cross-section dimensions and length) with "appropriate" (local and distortional) critical buckling loads. In order to shed new light on these coupling behavior, three simply supported columns sharing the aforementioned behavior are considered, namely (i) one experiencing "true L-D interaction", with $R_{DL}=P_{crd}/P_{crl}\approx 1.00$, and (ii) two affected by "secondary-bifurcation L-D interaction", (ii_1) one exhibiting a "secondary local bifurcation" ($R_{DL}\approx 0.60$) and (ii_2) the other a "secondary distortional bifurcation" ($R_{DL}\approx 1.60$). As done in previous studies, this geometry selection was made by means of a "trial-and-error" procedure involving the performance of GBT buckling analysis sequences using the code GBTUL (Bebiano *et al*. 2008) and including all conventional deformation modes. Table 1 shows the output of this effort, *i.e.*, the cross-section dimensions (b_w, b_f, b_l, t – web-flange-lip widths and wall thickness) of the three columns (E=210GPa, ν=0.3) selected to be analyzed. On the other hand, Figs. 2(a)-(c) show curves providing the variation of P_{cr} (critical buckling load) with the column length L (logarithmic scale) for the lipped channel (C-section) columns – Figs. 2(a)-(c) concern the columns with $R_{DL}\approx 0.60$, 1.00 and 1.60, respectively. Marked on these curves is the selected lengths adopted to ensure the desired interaction "levels". The critical local and distortional buckling loads and the corresponding buckling mode half-wave numbers (n_l and n_d) are also given in Table 1 (the buckling mode shapes are also

depicted in Figs. 2(a)-(c)). In order to ensure that no interaction with global (flexural-torsional) buckling occurs, these columns have global critical buckling loads much higher than their local and distortional counterparts – the relatively short lengths adopted automatically satisfy this criterion.

Table 1: Lipped channel column selected geometries, local and distortional buckling loads and buckling mode critical half-wave numbers (dimensions in mm and loads in kN)

Column	b_w	b_f	b_l	t	L	P_{crD}	P_{crL}	R_{DL}
1	100	80	10	1.90	400	107.6(1)	179.3(5)	0.60
2	120	80	10	1.36	450	51.8(1)	52.3(5)	1.00
3	120	80	15	1.36	500	86.0(1)	53.6(5)	1.60

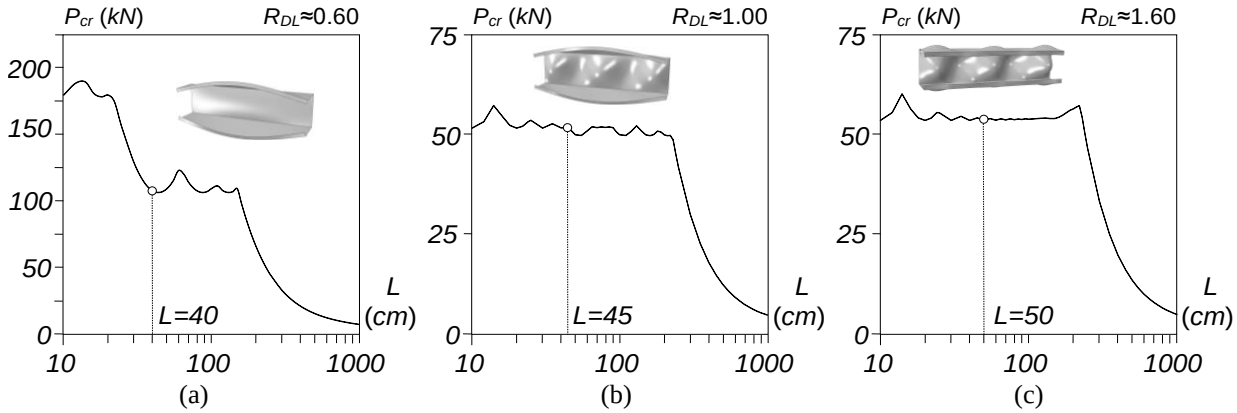

Figure 2: Lipped channels columns: P_{cr} vs. L curves, selected lengths and corresponding critical buckling mode shapes.

4. Column Post-Buckling Behavior Affected by Local-Distortional Interaction

The column geometries previously selected are used to investigate the influence of L-D interaction in the structural response of those columns, by means of GBT geometrically non-linear imperfect analyses (GNIA), with the aim of shedding fresh light on the mechanical aspects involved in the post-buckling behavior of simply supported columns (end cross-sections pinned and free to warp). The compressive force is applied at both end cross-sections, where the mode **1** displacements (axial extension) are free to occur – they are prevented at the mid-span cross-section, thus ensuring that the loading and support conditions are "fully symmetric"[6]. The results concerning the column experiencing "true L-D interaction" are addressed first (Section 4.1), after which are presented the results of the columns affected by "secondary-bifurcation L-D interaction" (Section 4.2). All the columns analyzed contain (i) critical-mode initial geometrical imperfections with small amplitudes (10% of the wall thickness t) and (ii) are longitudinally discretized into 24 GBT-beam finite elements. The GBT-based results are compared with values yielded by shell finite element analyses (SFEA) carried out in the code ABAQUS (Simulia Inc 2008), employing models already adopted in previous L-D interaction studies (*e.g.*, Dinis *et al*. 2007).

4.1 True L-D Interaction

Figure 3 display the L-D post-buckling equilibrium paths P/P_{cr} vs. v/t (v is the mid-span top flange-lip corner vertical displacement caused by the applied load, *i.e.*, excluding the value stemming from the

[6] Silvestre & Camotim (2004c) showed that, at the advanced post-buckling stages, the adoption of the other possible loading and support conditions rigid-body axial conditions (compressive force applied at one end cross-section only, while the other end cross-section is restrained against the axial rigid-body motion) has a non-negligible impact on the column deformed configuration.

initial geometrical imperfection) of the simply supported lipped channel columns, as well as the shape of the initial geometrical imperfections adopted. Since Dinis *et al*. (2007) and Dinis & Camotim (2015) showed that a "pure" distortional initial geometrical imperfection involving outward flange-lip motions corresponds to the lowest column strengths in C columns, these shapes were included in the GBT-based GNIA carried out in this work[7] – these columns exhibit a non-negligible post-buckling asymmetry, regarding the "sign" of the flange-lip motions, which was first unveiled by Prola & Camotim (2002). The GBT buckling analysis provides the following modal participations: **5**-89%, **7**-9%, **9**-2%. In order to highlight the relative importance of the different deformation modes on the column structural response, five "approximate analyses" were performed, namely those including the following deformation mode sets: (i) **1**+**5**, (ii) **1**+**3**+**5**, (iii) **1**+**3**+**5**+**7**+**9**, (iv) **1**+**3**+**5**+**7**+**9**+**15**+**17**, and (v) **1**+**3**+**5**+**7**+**9**+**15**+**17**+**26**.

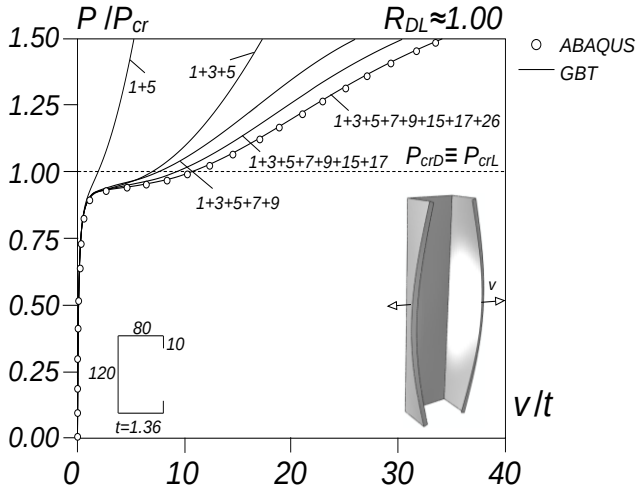

Figure 3: GBT-based post-buckling equilibrium paths of the lipped channel column undergoing "true L-D interaction" and obtained with different deformation mode sets.

The curves displayed in Figs. 4(a)-(d) provided the evolution, as P/P_{cr} increases from P/P_{cr}=0.75 (fairly advanced loading stages) of the web transverse displacement (w) profiles caused by the contributions of modes **3** (Fig. 4(a) – $w_3(x)$), **5** (Fig. 4(b) – $w_5(x)$), **7**+**9** (Fig. 4(c) – $w_{7+9}(x)$)[8] and **3**+**5**+**7**+**9** (Fig. 4(d) – $w_{3+5+7+9}(x)\equiv w(x)$). On the other hand, Figs. 5(a)-(b) concern earlier loading stages and depict the evolution of $w_{7+9}(x)$ between P/P_{cr}=0.25 and P/P_{cr}=0.75. Finally, Fig. 6 shows column deformed configurations at several advanced loading/post-buckling stages, namely for P/P_{cr}=1.00; 1.17; 1.33; 1.50. The analysis of all these post-buckling results prompts the following remarks:

(i) The GBT equilibrium path obtained with the **1**+**3**+**5**+**7**+**9**+**15**+**17**+**26** deformation mode set virtually coincides with the SFEA ("exact") one up to P/P_{cr}=1.50 – note that failure occurs for P/P_{cr}=1.77.

(ii) The adoption of the conventional deformation mode set (**1**+**3**+**5**+**7**+**9**) leads to accurate equilibrium paths only up to $P/P_{cr}\approx$0.90. Beyond this applied load level, the accuracy of the GBT response improves with the inclusion of the shear modes (**15**+**17**), but only the further inclusion of the transverse extension mode **26** makes it possible to "match" the SFEA equilibrium path.

[7] The above studies also consider various critical-mode initial geometrical imperfections combining arbitrarily normalized local and buckling mode shapes, obtained with SFEA, and sharing the same overall amplitude (10% of the wall thickness t).

[8] In order to "capture" the contribution of local deformations to the web transverse bending displacement profile – note that local buckling is triggered by the web in these columns. At this point, it is worth recalling that the column critical "distortional" buckling mode exhibits a 11% contribution from the local modes **7**+**9**. This means that part of the $w_{7+9}(x)$ displacement profile "belongs" to the single half-wave "distortional" deformations.

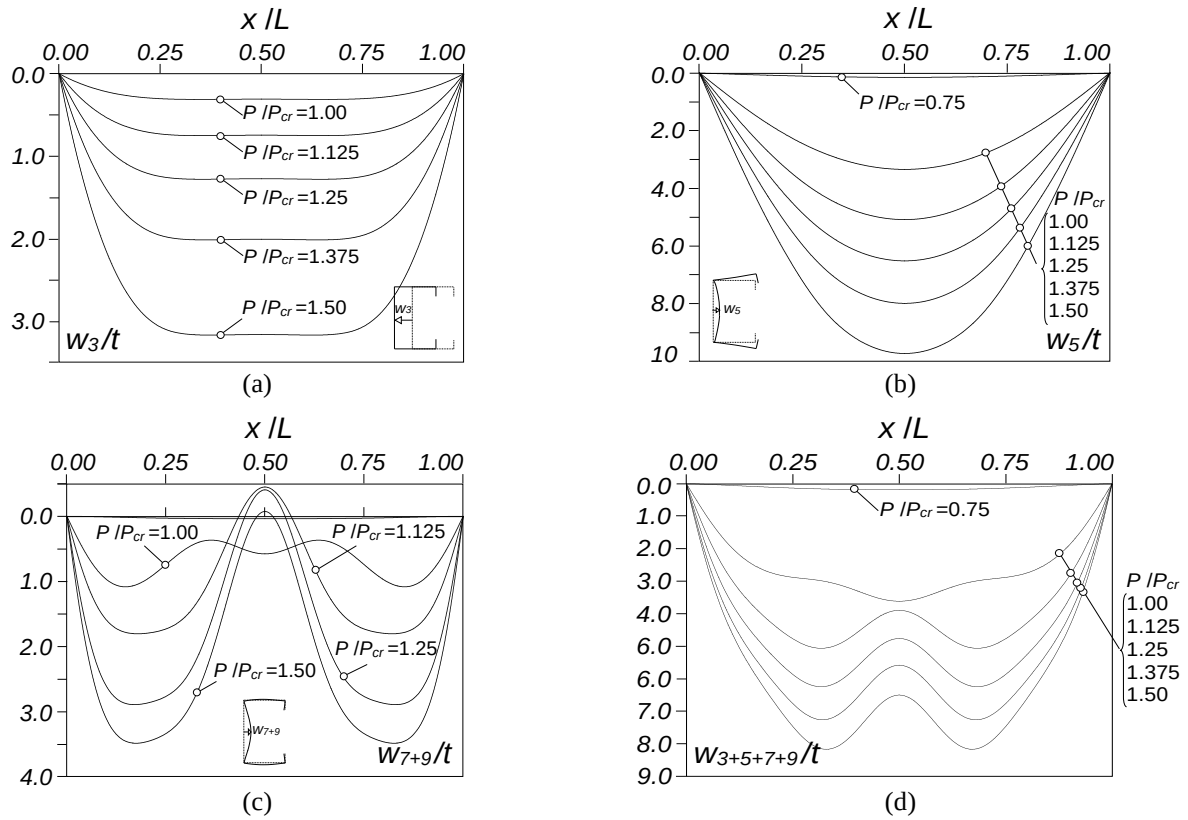

Figure 4: Evolution of the web transverse bending displacement profile caused by the deformation modes (a) **3** ($w_3(x)$), (b) **5** ($w_5(x)$), (c) **7+9** ($w_{7+9}(x)$) and (d) **3+5+7+9** ($w_{3+5+7+9}(x) \equiv w(x)$), for the column with R_{DL}=1.00.

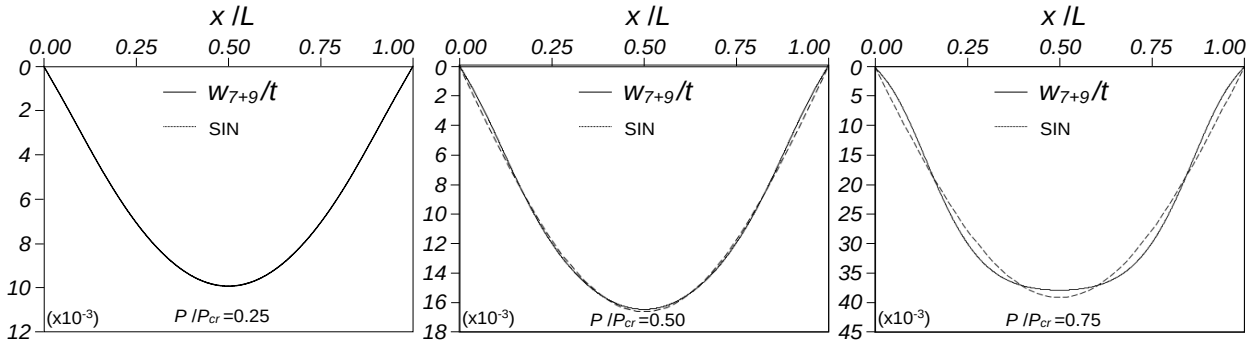

Figure 5: Contribution of the local deformation modes **7+9** ($w_{7+9}(x)$) to the web transverse bending of the column with R_{DL}=1.00 for (a) P/P_{cr}=0.25, (b) P/P_{cr}=0.50 and (c) P/P_{cr}=0.75.

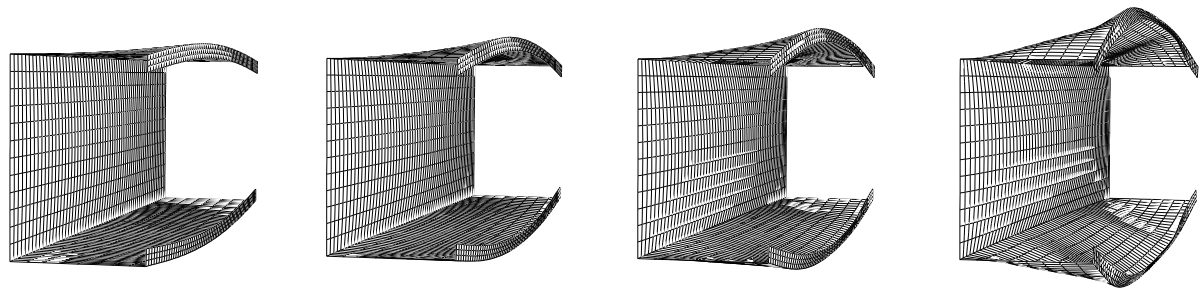

P/P_{cr}=1.00 P/P_{cr}=1.17 P/P_{cr}=1.33 P/P_{cr}=1.50

Figure 6: C column ABAQUS deformed configurations for P/P_{cr} =1.00; 1.17; 1.33; 1.50 (R_{DL}=1.00).

(iii) The observation of Figs. 5(a)-(c), which include purely sinusoidal curves for comparison purposes, shows that the web transverse displacement profile $w_{7+9}(x)$, quantifying the contribution of the local deformation modes, (iii_1) is virtually sinusoidal for $P/P_{cr}\approx0.25$ and (iii_2) gradually moves away from this shape as the loading increase to $P/P_{cr}\approx0.50$ and $P/P_{cr}\approx0.75$. A closer look at the differences between $w_{7+9}(x)$ and the sinusoidal curve shows that these differences exhibit five half-waves, *i.e.*, are akin to the columns critical *local* buckling mode. This emergence of deformations akin to the local buckling mode at early loading stages characterizes the so-called "true L-D interaction" and implies that this coupling phenomenon would also occur in an elastic-plastic column regardless of its yield stress (provided, of course, that the squash load P_y is not extremely below P_{cr}).

(iv) Figures 4(a)-(d) concern higher applied load levels ($P/P_{cr}\geq0.75$) and show that, for $P/P_{cr}=1.0$, the web transverse displacement longitudinal profile $w(x)\equiv w_{3+5+7+9}(x)$ consists of a combination of the following three modal contributions: (iv_1) a dominant distortional (mode **5**) single half-wave sinusoid, akin to the initial imperfection shape (see Fig. 4(b)), (iv_2) a local (modes **7**+**9**) five unequal half-wave curve, now clearly visible, and (iv_3) a global minor-axis flexure (mode **3**) curve "flattened" in the column central region, which stems from the load eccentricity caused by the effective centroid shift due to the stress redistribution associated with the pronounced web transverse bending (Young & Rasmussen 1999) – note that the curve is "flattened" because the load eccentricity is fairly uniform in the column central region. When the loading increases beyond $P/P_{cr}=1.0$, the above picture changes slightly, due to the fact that the shape of the local mode contribution suddenly "snaps" from five half-waves to three-half-waves: the three fairly small internal half-waves abruptly merge into a single large one so large that it entails negative local displacement values in the vicinity of the column mid-span for $P/P_{cr}=1.125$ – these negative values are subsequently attenuated as the loading progresses up to $P/P_{cr}=1.50$[9]. For $P/P_{cr}>1.125$, the contribution of the GBT local deformation modes to $w(x)$ (not included in the critical buckling mode shape) becomes clearly visible in Fig. 5(d).

(v) It should be noted that considering a different initial imperfection shape (*e.g.*, a "pure" local buckling mode shape) may change considerably the evolution of $w(x)$, particularly at the earlier loading stages – the changes become progressively less meaningful as the loading progresses (Dinis *et al.* 2007).

Finally, Fig. 7 provides the evolution of the mid-span membrane longitudinal normal stress distribution as the uniform applied load level P/P_{cr} increases. The following conclusions can be drawn from the observation of these stress diagrams:

(i) At the early loading stages, the stress diagram remais pratically uniform, since mode **1** (axial extension) is practically the only one participating in the column deformed configuration.

(ii) As loading progress, the compressive normal stresses gradually (ii_1) increase in the lips, exhibiting a linear variation that reaches very high values in the free at the more advanced post-buckling stages (these very high lip compressive stresses are responsible for reducing the column strength), (ii_2) increase in the flange-web corners and (iii_3) deacrease in the lip-flange corners where tensile strsses develop, even at relatively early loading stages – these evolution are due the growing contibutions of deformation modes **5** (mostly – it exhibits a strong warping displacement linear variation at the lips), **15** and **17**. Moreover, due to the increasing stress redistribution associated with the (local) post-buckling behavior associated with wall transverse bending, stress diagram developing in the web becomes clearly non-linear for $P/P_{cr}>0.90$.

[9] No clear physical explanation could yet be found for this "snapping" (local mode switch) phenomenon. It may be due to the coupling (either structural or "numerical" – "jump" to a neighboring equilibrium state) between local buckling modes with three and five half-waves – the corresponding column buckling loads are very close to each other.

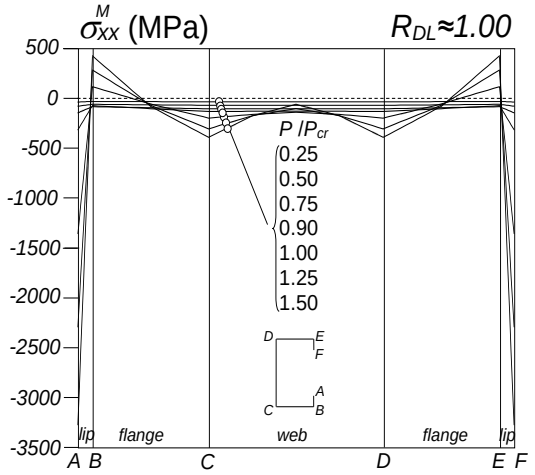

Figure 7**:** Evolution of the mid-span membrane normal longitudinal stress distribution for the column with R_{DL}=1.00.

(iii) In previous work (Martins *et al*. 2014a,b), the authors observed that, in columns experiencing "true L-D interaction", the onset of yielding always occurs at the lip free ends of the "most distorted" wave exhibiting outward flange-lip motions – this observation is in agreement with the very high compressive stress mentione in the previous item and shown the relevant role played by the distortional deformations in the column elastic-plastic behavior (and eventual collapse).

(iv) The normal stress distribution patterns obtained for these columns are qualitatively similar to those reported by Silvestre & Camotim (2006) for a "pure"/individual distortional post-buckling behavior – note the extremely high compresive stresses occurring at the lips free ends, due to mode **5**, much larger than those acting on the remaining of the cross-section, due to modes **5**+**7**+**9**. Naturally, the consideration of a local initial imperfection shape would lead to a different stress evolution at the early loading stages – however, as loading progresses, the influence of the fast growing contribution of the distortional mode **5** leads to stress distributions similar to those shown in Fig. 7.

4.2 Secondary-Bifurcation L-D interaction

4.2.1 Secondary Local Bifurcation

First of all, it is worth mentioning that the type of results presented in this Section, concerning the R_{DL}=0.60 column characterized in Table 1, is similar to those reported in Section 4.1. Therefore, the corresponding descriptions and discussions are abbreviated whenever possible. Figure 8 shows the post-buckling equilibrium paths P/P_{cr} vs. v/t and the initial geometrical imperfection shape included in the GBT analyses performed, which consists again of the distortional critical buckling mode shape involving outward flange-lip motions – a GBT buckling analysis showed that this buckling mode exhibits visible contributions from deformation modes **5**-93%, **7**-5%, **9**-1% (note that the distortional mode is "more dominant" than in the previously analyzed column). In order to assess the relevance of the different GBT deformation modes for the column response, the equilibrium paths displayed in Fig. 8 were obtained by means of GBT analyses including the deformation mode sets (i) **1**+**5**, (ii) **1**+**3**+**5**, (iii) **1**+**3**+**5**+**7**+**9**, (iv) **1**+**3**+**5**+**7**+**9**+**15**+**17**, and (v) **1**+**3**+**5**+**7**+**9**+**15**+**17**+**26**. As before, Figs. 9(a)-(d) and 10 show, respectively, (i) the evolution of the web transverse displacement longitudinal profiles stemming from the contributions of modes **3** (Fig. 9(a) – $w_3(x)$), **5** (Fig. 9(b) – $w_5(x)$), **7**+**9** (Fig. 9(c) – $w_{7+9}(x)$) and **3**+**5**+**7**+**9** (Fig. 9(d) – $w_{3+5+7+9}(x)\equiv w(x)$), and (ii) web flexural deformed configurations for P/P_{cr}=1.00; 1.25; 1.50; 1.75. The close observation of the results presented in these figures leads to the followings conclusions:

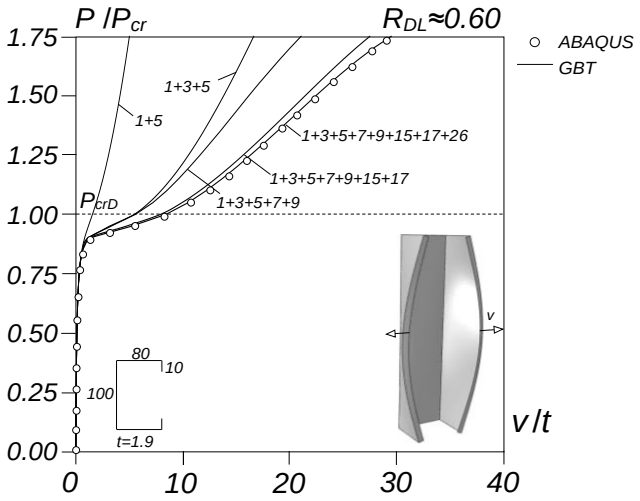

Figure 8: GBT-based post-buckling equilibrium paths of the lipped channel column undergoing "Secondary local bifurcation L-D interaction" and obtained with different GBT deformation mode sets.

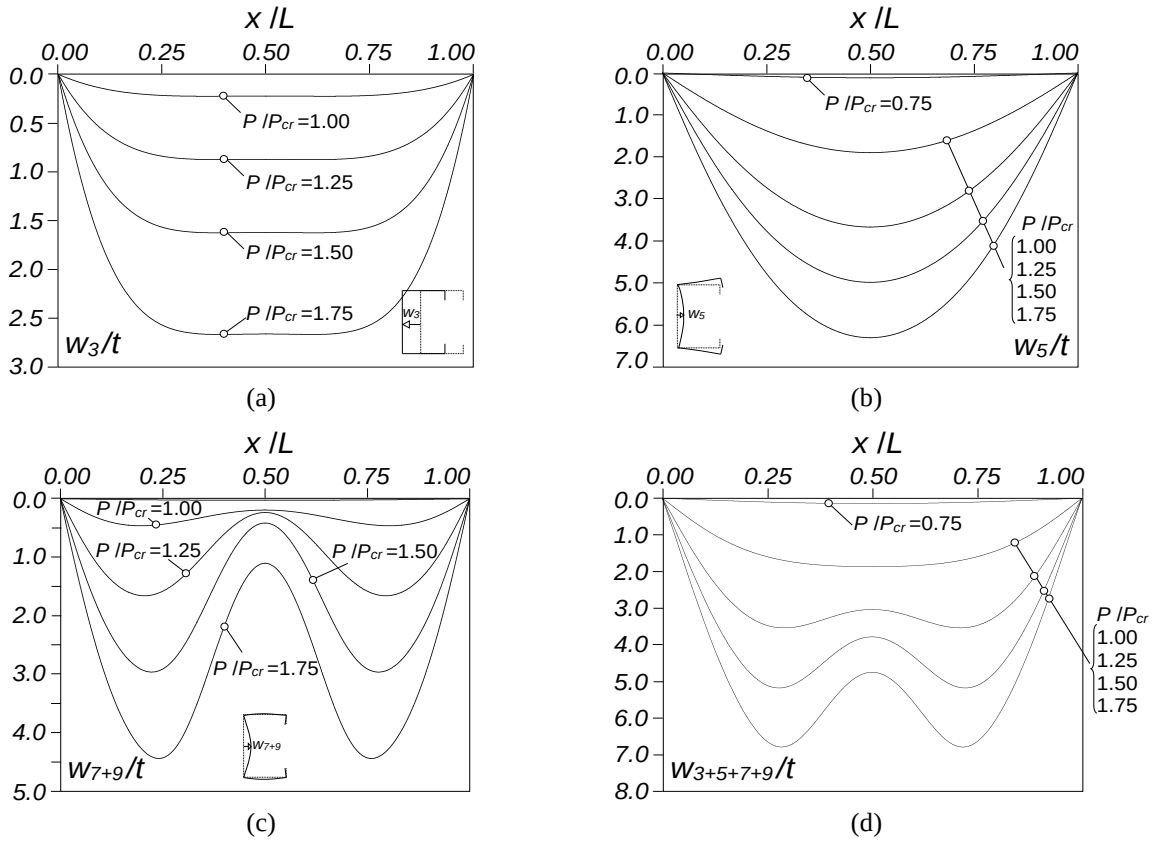

Figure 9: Evolution of the web transverse bending displacement profile caused by the deformation modes (a) **3** ($w_3(x)$), (b) **5** ($w_5(x)$), (c) **7+9** ($w_{7+9}(x)$) and (d) **3+5+7+9** ($w_{3+5+7+9}(x)\equiv w(x)$), for the column with R_{DL}=0.60.

(i) The equilibrium path obtained with the **1**+**3**+**5**+**7**+**9**+**15**+**17**+**26** virtually coincides with the "exact" ABAQUS SFEA one up to P/P_{cr}=1.75. This is particularly striking, since the GBT analysis involves only 456 d.o.f., a tiny fraction of the number required by the SFEA (over 27000 d.o.f.). Moreover, note that this is exactly the same mode deformation combination set that led to "exact" results for the column analyzed in Section 4.1.

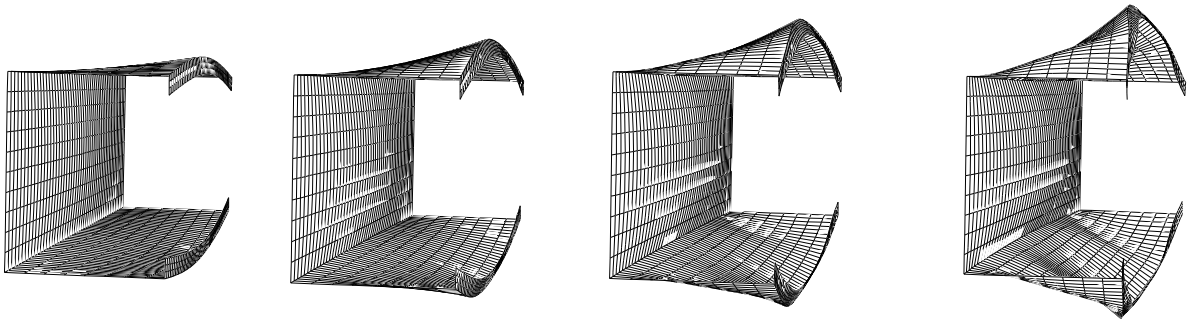

P/P_{cr}=1.00 P/P_{cr}=1.25 P/P_{cr}=1.50 P/P_{cr}=1.75

Figure 10: ABAQUS C column deformed configurations for P/P_{cr}=1.00; 1.17; 1.33; 1.50 (R_{DL}=0.60).

(ii) As before, the consideration of only the conventional modes **1**+**3**+**5**+**7**+**9** leads to very accurate results up to $P/P_{cr}\approx0.90$, an applied load level beyond which it is necessary to include the shear modes **15**+**17** and the transverse extension mode **26** to obtain similarly accurate values.

(iii) Up until P/P_{cr}=0.75, $w(x)$ exhibits a clear single half-wave that combines (iii$_1$) a dominant distortional (mode **5**) single half-wave sinusoid and (iii$_3$) a global minor-axis flexure (mode **3**) curve, again "flattened" in the column central region (effective centroid shift effect) – no trace of a five half-wave local deformation mode contribution is detectable[10].

(iv) For P/P_{cr}=1.00, $w(x)$ already exhibits a visible three half-wave local deformation mode contribution, even if the column critical local buckling mode has five half-waves[11]. When the loading increases beyond P/P_{cr}=1.0, the picture does not change up to P/P_{cr}=1.75 – only a steady growth of the various displacement amplitudes is observed. The emergence of deformations akin to local buckling modes at only at relatively advanced loading stages characterizes the so-called "secondary local bifurcation L-D interaction" and implies that this coupling phenomenon does not occur in an elastic-plastic column if its squash load P_y is moderately below P_{cr}[12].

Lasty, Fig. 11 displays the evolution of the mid-span membrane longitudinal normal stress distribution for different applied load levels P/P_{cr}. In view of the strong resemblance between these stress distributions and those presented in Fig. 7 ("true L-D interaction"), all the comments made earlier remain valid both qualitatively and quantitavely (almost).

4.2.2 Secondary Distortional Bifurcation

Figure 12 shows the post-buckling equilibrium path P/P_{cr} vs. w/t (w is the mid-span web mid-point transverse displacement caused by the applied load) and the initial geometrical imperfection shape inclued in the GBT-based GNIA. Unlike in the two columns analyzed previously, critical-mode initial

[10] An investigation similar to the one reported for the column analyzed in Section 4.1 confirmed the absence of these local deformations up until P/P_{cr}=0.75 – indeed the web transverse bending displacement profile perfectly matches a half-wave sinusoid up to this applied load level.

[11] A more refined analysis, carried out for applied loads between P/P_{cr}=0.75 and P/P_{cr}=1.0 showed that a perceptible local deformation mode contribution only emerges for P/P_{cr}=0.85 and exhibits five half-waves. This means that a "snapping" (local mode switch) phenomenon, similar to the one observed for the R_{DL}=1.00 column, occurs between prior to P/P_{cr}=1.0.

[12] Martins *et al.* (2014a,b) recently analyzed several fixed-ended columns with $R_{DL}\approx0.60$ and showed that, even when the ratio P_y/P_{cr} is quite large, the influence of the L-D interaction on the column failure loads is minute, as attested by the fact that these loads are accurately predicted by the currently codified Direct Strength Method (DSM) distortional design curve – only for columns with R_{DL}>0.80 does L-D interaction erodes the column ultimate strength. In the simply supported column analyzed in this work, the equilibrium path exhibits a limit point that takes place at P/P_{cr}=1.74, very soon after the "secondary-bifurcation" load level (P/P_{cr}=1.66), which means that, in elastic-plastic columns, the failure load erosion is never expected to be significant.

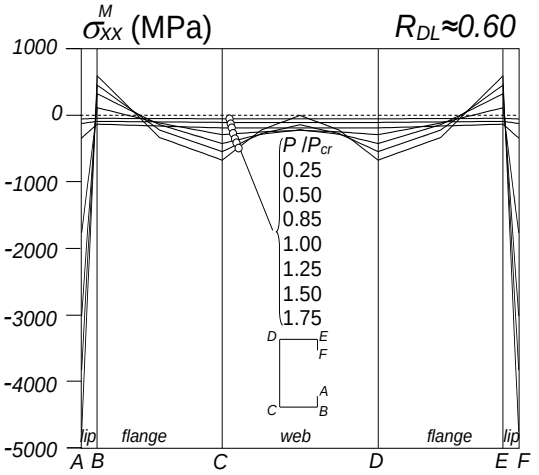

Figure 11: Evolution of the mid-span membrane normal stress distribution for the C R_{DL}=0.60 column.

imperfection shape is local, exhibits five half-waves and involves inward web bending at mid-span. The GBT buckling analysis provided the following most relevant modal participations factors: **7**-88%, **9**-9%, **5**-1% – because of the last (minute) contribution, the mode **5** amplitude function $\phi_5(x)$ displays now five half-waves at the early loading stages (not shown here). This equilibrium path was obtained with the GBT deformation mode set **1**+**3**+**5**+**7**+**9**+**15**+**17**+**19**+**26**, which leads to extremely accurate results – see the comparison with the "exact" SFEA equilibrium path up to P/P_{cr}=1.75[13].

The curves depicted in Figs. 13(a)-(d) provide the evolution, as P/P_{cr} increases from P/P_{cr}=0.50, of the web transverse bending displacement (w) profiles caused by the contributions of modes **3** (Fig. 13(a) – $w_3(x)$), **5** (Fig. 13(b) – $w_5(x)$[14]), **7**+**9** (Fig. 13(c) – $w_{7+9}(x)$) and **3**+**5**+**7**+**9** (Fig. 13(d) – $w_{3+5+7+9}(x)\equiv w(x)$). Finally, Fig. 14 shows column deformed configurations (amplified 5 times) at four loading levels, namely P/P_{cr}=1.00; 1.25; 1.50; 1.75 (all corresponding to quite advanced post-buckling paths stages). The close observation of all these post-buckling results leads to the following comments:

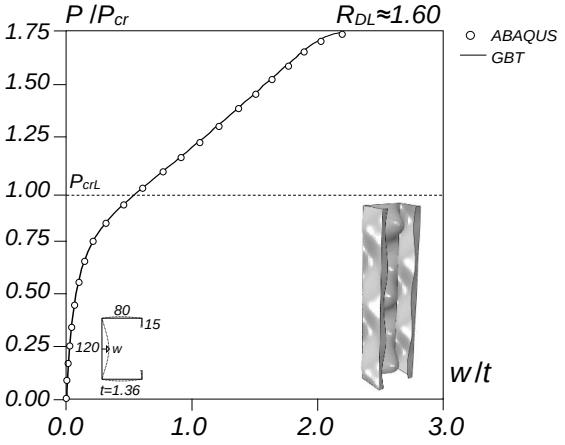

Figure 12: GBT-based post-buckling equilibrium path of the lipped channel column undergoing "Secondary distortional bifurcation L-D interaction".

[13]Note that the equilibrium path limit point takes place for P/P_{cr}≈1.77, *i.e.*, again quite soon after the "secondary-bifurcation" load level (P/P_{cr}≈1.60). This behavioral feature, which also occurred in the column with a "secondary local bifurcation", implies that, in elastic-plastic columns, the failure load will never be much influenced by L-D interaction – if the squash load exceeds visibly the critical distortional bifurcation one, the column fails either elastically or very soon after the onset of yielding.

[14]In order to enable capturing the contribution of mode **5** (distortional deformation) to the web transverse bending displacements.

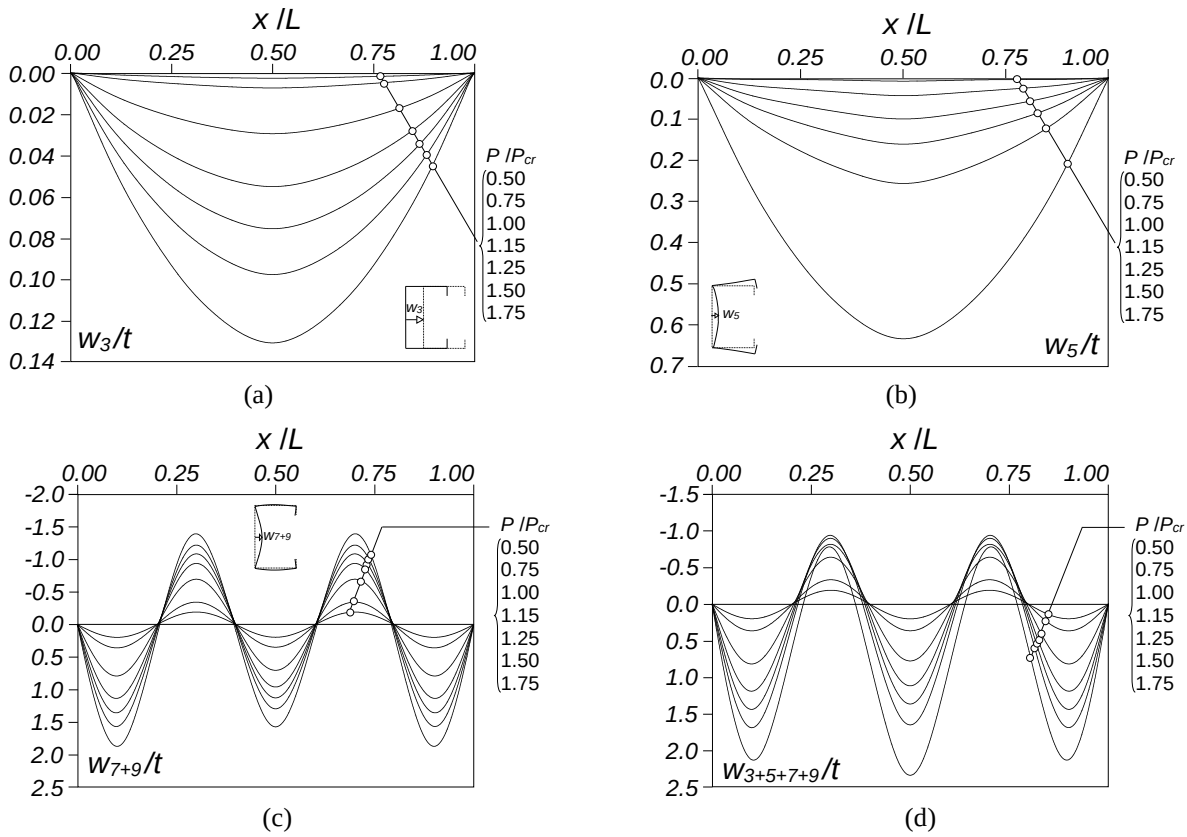

Figure 13: Evolution of the web transverse bending displacement profile caused by the deformation modes (a) **3** ($w_3(x)$), (b) **5** ($w_5(x)$), (c) **7+9** ($w_{7+9}(x)$) and (d) **3+5+7+9** ($w_{3+5+7+9}(x)\equiv w(x)$), for the column with R_{DL}=1.60.

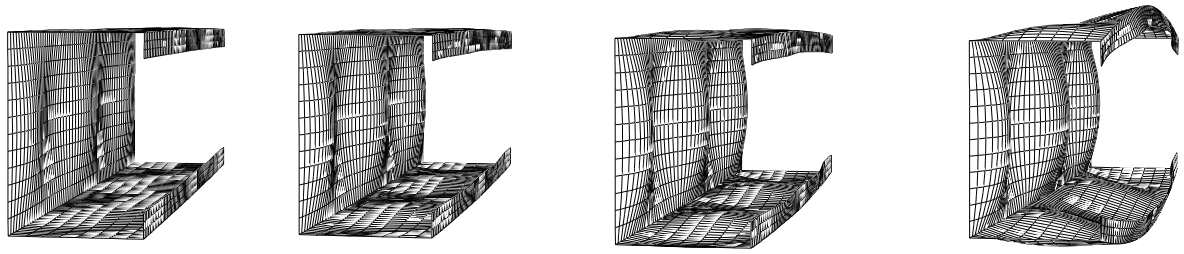

P/P_{cr}=1.00 P/P_{cr}=1.25 P/P_{cr}=1.50 P/P_{cr}=1.75

Figure 14: Column ABAQUS deformed configuration for P/P_{cr}=1.00; 1.25; 1.50; 1.75 (R_{DL}=1.60) – all amplified 5 times.

(i) For $P/P_{cr}\leq 0.75$, the web displacement longitudinal profile $w(x)\equiv w_{3+5+7+9}(x)$ shown in Fig. 13(d) consists almost exclusively of the five half-wave contribution of the local deformation modes **7**+**9**, akin to the initial imperfection shape – the single half-wave contributions from modes **3** and **5**, shown in Figs. 13(a)-(b), are barely visible (the amplitudes of the five half-waves are fairly identical). When loading increases beyond P/P_{cr}=0.75, the above picture begins to change, as the relative importance of the contributions of modes **3** and **5** (mostly the second one) gradually grow[15], which is evidenced by the fact that the five half-waves of $w_{3+5+7+9}(x)$ become progressively more unequal: the central half-wave amplitude increases beyond the remaining ones, while the two adjacent half-waves decrease, thus reflecting the presence of the aforementioned single half-wave modal contributions – this is very clearly visible, both in Figs. 13(d) and 14, for P/P_{cr}=1.75, *i.e.*, just before the ultimate load.

[15]Naturally, the loading state associated with the emergence of the distortional depends on the column R_{DL} value.

The emergence of the distortional deformations at fairly advanced loading stages (close to P/P_{cr}=1.0), characterizes the so-called "secondary distortional bifurcation L-D interaction" and means that this interactive behavior does not occur in an elastic-plastic column if its squash load P_y is below its critical buckling load P_{cr}. Indeed, these deformations can only emerge visibly if the squash load yield is large enough to allow the applied load to approach the distortional bifurcation load level, taking advantage of the high column local post-critical strength reserve.

(ii) It is interesting to notice that the mode **3** amplitude function now resembles a lot a single-half-wave sinusoid, which did not happen in the two columns analyzed previously (this amplitude function had a "flattened" central portion). Although no clear physical explanation for this difference was yet unveiled, it has certainly to do with the fact that the effective centroid shift now stems primarily from local deformations (and not distortional ones, as before).

5. Concluding Remarks

A numerical investigation concerning the geometrically non-linear response of simply supported thin-walled lipped channel columns experiencing local-distortional (L-D) interaction was reported in this paper. The results presented and discussed, which were obtained through GBT post-buckling analyses and validated through the comparison with ABAQUS SFEA values, provided the evolution, along given equilibrium paths, of the column (i) deformed configuration, expressed in modal form, and (ii) relevant displacement profiles and stress distributions. Particular attention was paid to the structural interpretation of the behavioral features that characterize the column post-buckling behaviors associated with the three types of L-D interactive behavior, namely (i) "true", (ii) "secondary local bifurcation" and (iii) "secondary distortional bifurcation" interaction.

Initially, GBT buckling analyses were performed to identify columns exhibiting the three distinct L-D interactive behaviors mentioned in the previous paragraph – column C1 (almost coincident critical local and distortional buckling loads, column C2 (critical distortional buckling load lower than its local counterpart) and column C3 (critical distortional buckling load higher than its local counterpart). Then, the paper presented and discussed in great detail the results of geometrically non-linear imperfect analyses of the above three columns, all containing critical-mode initial geometrical imperfections with small amplitude. Web transverse bending displacement profiles, influenced by both local and distortional deformations, were the vehicle used to shed fresh light on the evolution of the relative importance of those two types of deformation as loading progresses – the "core business" of L-D interaction.

Among the various conclusions drawn from this investigation, the following ones deserve to be specially noted, as they concern the most relevant behavioral/mechanical features characterizing the occurrence of the aforementioned three types of L-D interaction:

(i) First of all, the three columns exhibit L-D interaction, in the sense that deformations patterns akin both the local and distortional critical buckling modes occur prior to the failure load. However, it was also unveiled that the relevance of L-D interaction is markedly different in (i_1) column C1 ("true L-D interaction") and (i_2) columns C2 and C3 ("secondary-bifurcation L-D interaction").

(ii) In column C1, analyzed with distortional critical-mode initial imperfections, deformations akin to the (also critical) local buckling mode emerged at early loading stages and significantly increased up until the failure load[16], which occurred about 75% above the critical load level. This means that L-D

[16] Note that, since all the columns were analyzed in the elastic regime, the corresponding failure loads stem exclusively from geometrically non-linear effects.

interaction occurs along practically the whole column equilibrium path ascending branch, which extends well beyond the critical load level. Therefore, in elastic-plastic columns and regardless of the yield stress value (except, of course, the squash load is extremely below P_{cr}), there is always some (more or less) "room" for L-D interaction to develop and erode of the column failure load.

(iii) In column C2, also analyzed with distortional critical-mode initial imperfections, deformations akin to the (non-critical) local buckling mode emerged at relatively advanced loading stages and only mildly increased before the failure load, which occurred very soon after the secondary local bifurcation load level. Therefore, in elastic-plastic columns, there is never significant L-D interaction prior to failure, which means that the column failure will be predominantly distortional, with no visible failure load erosion caused by the above coupling phenomenon – the columns just have to be designed against distortional failures.

(iv) In column C3, analyzed with local critical-mode initial imperfections, the situation is similar to that of column C2, if the words "local" and "distortional" are switched. Indeed, deformations akin to the (non-critical) distortional buckling mode emerged at fairly advanced loading stages and only marginally increased before the failure load, occurring again very soon after the secondary bifurcation load level (now distortional). Thus, in elastic-plastic columns, there also never significant L-D interaction prior to failure and, therefore, the column failure will be predominantly local, once more with no visible failure load erosion due to the interactive behavior – now, the columns just have to be designed against local failures.

(v) In view of what was mentioned in the previews three items, it seems fair to conclude that, in simply supported lipped channel columns, only "true L-D interaction" is relevant for practical purposes, as both "secondary-bifurcation L-D interaction" behaviors were found to have very little (if any) effect on the column failure load. This fact has important practical implications and contrasts with the findings recently reported for fixed-ended lipped channel columns by the authors (Martins *et al.* 2014a), who employed ABAQUS SFEA results to show that, depending on how high the yield stress is, the presence of "secondary-bifurcation L-D interaction" may lead to a significant failure load erosion (particularly when local buckling precedes distortional buckling). This is due to the very high distortional post-critical strength reserve increase caused by fixing the column end cross-sections – *e.g.*, no elastic limit point was ever detected in fixed-ended lipped channel columns analyzed well beyond the secondary bifurcation load level.

(vi) At this point, it is worth mentioning that the authors are currently undergoing a GBT-based investigation similar to that reported in this paper for fixed-ended lipped channel columns. It is known that, due to the added distortional post-critical strength reserve, the extent and relevance of the three types of L-D interaction dealt with here is considerably higher than for the simply supported columns – the GBT results will surely provide in-depth insight on this marked behavioral difference.

Acknowledgments

The first and fourth authors gratefully acknowledge the financial support of FCT (*Fundacão para a Ciência e a Tecnologia* – Portugal), through the (i) doctoral scholarship SFRH/BD/87746/2012 and (ii) project grant Pest-C/EEI/UI0308/2011, respectively.

References

Basaglia C, Camotim D, Silvestre N (2011). Non-linear GBT formulation for open-section thin-walled members with arbitrary support conditions", *Computers & Structures*, **89**(21-22), 1906-1919.

Basaglia C, Camotim D, Silvestre N (2013). Post-buckling analysis of thin-walled steel frames using generalized beam theory (GBT), *Thin-Walled Structures*, **62**(January), 229-242.

Basaglia C, Landesmann A, Camotim D (2014). About the influence of the cross-section geometry on the distortional post-buckling strength of cold-formed steel columns", *Proceedings of SSRC Annual Stability Conference* (Toronto, 25-28/3).

Bebiano R, Silvestre N, Camotim D (2005). Buckling and post-buckling behaviour of stiffened cold-formed steel columns: a comparative study, *Proceedings of 4th European Conference on Steel and Composite Structures* (EUROSTEEL 2005 – Maastricht, 8-10/6), B. Hoffmeister and O. Hechler (eds.), 145-153 (part 1.2).

Bebiano R, Pina P, Silvestre N, Camotim D (2008). *GBTUL 1.0β – Buckling and Vibration Analysis of Thin-Walled Members*, DECivil/IST, Technical University of Lisbon. (*http://www.civil.ist.utl.pt/gbt*)

Clarke MJ, Hancock GJ (1990). A study of incremental-iterative strategies for non-linear analyses, *International Journal for Numerical Methods in Engineering*, **29**(7), 1365-1391.

Crisfield MA (2001). *Nonlinear Finite Element Analysis of Solids and Structures – Essentials* (Vol.1), John Wiley & Sons (Chichester).

Dinis PB, Camotim D (2015). Cold-formed steel columns undergoing local-distortional coupling: behaviour and direct strength prediction against interactive failure, *Computers & Structures*, **147**(January), 181-208.

Dinis PB, Camotim D, Silvestre N (2007). FEM-based analysis of the local-plate/distortional mode interaction in cold-formed steel lipped channel columns, *Computers & Structures*, **85**(19-20), 1461-1474.

Martins AD, Dinis PB, Camotim D, Providência P (2014a). On the relevance of local-distortional interaction effects in the behavior and design of cold-formed steel columns, *USB Proceedings of SSRC Annual Stability Conference* (Toronto, 25-28/3).

Martins AD, Dinis PB, Camotim D, Providência P (2014b). On the influence of local-distortional interaction in the behavior and design of cold-formed steel web-stiffened lipped channel columns", *Proceedings of 22nd International Specialty Conference on Cold-Formed Steel Structures* (CCFSS 2014, St. Louis, 5-6/9), 171-191.

Miosga G (1976). *Vorwiegend Längsbeanspruchte Dünnwandige Prismatische Stäbe und Platten mit Endlichen Elastischen Verformungen*, PhD dissertation, Technische Hochschule Darmstadt. (German)

Prola LC, Camotim D (2002). On the distortional post-buckling behavior of cold-formed lipped channel steel columns, *Proceedings of SSRC Annual Stability Conference* (Seattle, 24-27/4), 571-590.

Schardt R (1989). *Verallgemeinerte Technische Biegetheorie*, Springer-Verlag (Berlin). (German).

Simulia Inc. (2008), *ABAQUS Standard* (version 6.7-5).

Silva NMF (2013). *Behaviour and Strength of Thin-Walled Laminated FRP Composite Structural Elements*, Ph.D. Thesis in Civil Engineering, Technical University of Lisbon, Portugal.

Silva NMF, Camotim D, Silvestre N, Correia JR, Branco FA (2011). First-order, buckling and post-buckling behaviour of GFRP pultruded beams – Part 2: Numerical simulation, *Computers & Structures*, **89**(21-22), 2065-2078.

Silvestre N, Camotim D (2003). Nonlinear generalized beam theory for cold-formed steel members", *International Journal of Structural Stability and Dynamics*, **3**(4), 461-490.

Silvestre N, Camotim D (2004a). GBT-based analysis of the distortional post-buckling behaviour of cold-formed steel Z-section columns and beams, *Thin-Walled Structures: Advances in Research, Design and Manufacturing Technology* (ICTWS'04, Loughborough, 22-24/06), J. Loughlan (ed.), 243-250.

Silvestre N, Camotim D (2004b). Generalised beam theory formulation to analyse the post-buckling behavior of orthotropic laminated plate thin-walled members", *Proceedings of 21st International Congress of Theoretical and Applied Mechanics* (ICTAM'04 – Warsaw, 15-21/08), 345-346.

Silvestre N, Camotim D (2004c). GBT-based analysis of the local-plate/distortional buckling mode interaction in lipped channel columns, *Proceedings of 4th International Conference on Coupled Instabilities in Metal Structures* (CIMS'04 – Rome, 27-29/09), M. Pignataro, J. Rondal, V. Gioncu (eds.), Editura Orizonturi Universitare (Timisoara), 449-462.

Silvestre N (2005). *Generalized Beam Theory: New Formulations, Numerical Implementation and Applications*, Ph.D. Thesis in Civil Engineering, Technical University of Lisbon, Lisbon, Portugal. (Portuguese).

Silvestre N, Camotim D (2006). Local-plate and distortional postbuckling behavior of cold-formed steel lipped channel columns with intermediate stiffeners", *Journal of Structural Engineering* (ASCE), **132**(4), 529-540.

Silvestre N, Young B, Camotim D (2008). Non-linear behaviour and load-carrying capacity of CFRP-strenthened lipped channel steel columns, *Engineering Structures*, **30**(10), 2613-2630.

Young B, Rasmussen KJR (1999). Shift of effective centroid in channel columns, *Journal of Structural Engineering* (ASCE), **125**(5), 524-531.